

Hyper-sensitive piezophotovoltaic effects in ferroelectric nanocylinders

Yue Zheng^{a)} and C. H. Woo^{b)}

Department of Electronic and Information Engineering, The Hong Kong Polytechnic University, Hong Kong Special Administrative Region, China

(Received 10 January 2010; accepted 17 April 2010; published online 26 May 2010)

Photocurrent system of the ferroelectric nanocylinder (FNC), including nanodisks, nanorods, and nanowires, sandwiched between metal electrodes with the short-circuit boundary conditions has been designed and investigated. Taking into account the polarization charge screening in the electrodes and near-surface inhomogeneous polarization distribution, a theoretical model for investigating the photoinduced current of the FNC under the illumination of light was established. Our results show that the photocurrent of the FNC can be totally controlled by adjusting its size and states of the polarization “up” and “down.” Especially, reversing an applied stress can obviously change the photocurrent of the FNC, which is particularly significant near the stress-dependent para/ferroelectric phase transition. This piezophotovoltaic effect may have good potential for applications in high-sensitivity photomechanical sensors, memories, switchable nanodevices, or other photovoltaic nanodevices. © 2010 American Institute of Physics. [doi:10.1063/1.3428477]

I. INTRODUCTION

Ferroelectrics like BaTiO₃, LiNbO₃, PbTiO₃, PbZrTiO₃ (PZT), LiTaO₃, (PbLa)(ZrTi)O₃ (PLZT), BiFeO₃ (BFO), or (PbTiO₃)_x(BiFeO₃)_{1-x} (PTO_xBFO_{1-x}), etc.,¹⁻²³ are photovoltaic, and can produce a steady voltage or direct current when illuminated with ultraviolet (UV) or near-UV light. These materials have potential applications in many areas, such as optical microsensing, wireless actuation, microactuation in microelectromechanical systems, high-sensitivity photomechanical sensors (HSPMS), switchable nanodevices, nondestructive read out of memory, optoelectronic devices and optical information storage, etc. Historically, bulk photovoltaic effect has been observed in BaTiO₃ by Chynoweth as early as 1956,⁴ which was confirmed by Chen *et al.*⁵ in LiNbO₃ in 1969. Glass *et al.*⁶ introduced the Glass coefficient to characterize the bulk photovoltaic effect of the ferroelectrics, and established a relationship between the photocurrent density and light intensity. The most remarkable of the ferroelectric photovoltaic (FPV) effect is its high output voltage of over kilovolts. Recent experimental and theoretical works have established that among all known perovskite ferroelectric materials, (Pb_{0.97}La_{0.03}) × (Zr_{0.5}Ti_{0.5}O₃) (PLZT), or BFO could be the most promising candidates for photoelectric applications.¹⁶⁻²⁴

Photovoltaic effects occur generally in systems with asymmetric interfaces, such as semiconducting *p-n* junctions or metal-semiconductor interfaces with Schottky barriers.^{1-3,24-26} Both experimental and theoretical works have shown that the FPV effect is different from that in conventional *p-n* junctions or Schottky barriers of the semiconductors.¹⁸⁻²⁷ Although a complete understanding of the physical mechanisms involved in the FPV effect in

metal-ferroelectric-metal (MFM) structures with the short-circuit boundary conditions has not yet been accomplished, a widely accepted explanation of the photoelectric current is the separation of the photon-generated electron-hole pairs (excitons) by the internal electric field,²⁰⁻²⁴ which also provides the potential difference that drives the photocurrent in the external circuit connected to the ferroelectrics. In absence of an external electric field, the internal electric field comes from the depolarization field produced by polarization screening charges in the metal electrodes and the inhomogeneous polarization distribution near interfaces. Here the homogeneous polarization distribution is affected by complex factors,^{1,8,28-35} such as surface discontinuity of the ferroelectric layer,^{8,27,31,32} and Schottky barriers at interface, etc.^{10,14,27,29}

Theories and experiments on FNCs taking various forms such as nanodisks (ND), nanorods (NR), nanowires (NW), and nanotubes (NT) have indicated that their phase-transition or near-phase-transition properties are very sensitive to the applied stress.³³⁻⁴² In these investigations, stresses produced by surface tension and external mechanical loads have been found to significantly affect the Curie temperature, polarization, susceptibility and other related properties near the ferro/paraelectric phase transition, resulting in remnant polarization and coercive fields that may exceed the bulk values. Indeed, under an uniaxial load of suitable magnitude and frequency, an appropriately dimensioned ferroelectric NW may produce a sizeable ac voltage, sufficient as a nanopower source for energy harvesting, or as an effective nanomechanical sensor.^{41,42}

It is clear that FPV effects may become very small when the average internal electric field in FNC is zero.¹⁶⁻²⁴ In this case, the photocurrent is only due to charge transport via diffusion.

For the FNC with the short-circuit boundary conditions, the internal electric field is mainly due to the spontaneous polarization and interface effects, which is known to be very much affected by an applied mechanical load, particularly

^{a)}Present address: State Key Laboratory of Optoelectronic Materials and Technologies, Institute of Optoelectronic and Functional Composite Materials, and School of Physics and Engineering, Sun Yat-sen University, China. Electronic mail: zhengy35@mail.sysu.edu.cn.

^{b)}Electronic mail: chung.woo@polyu.edu.hk.

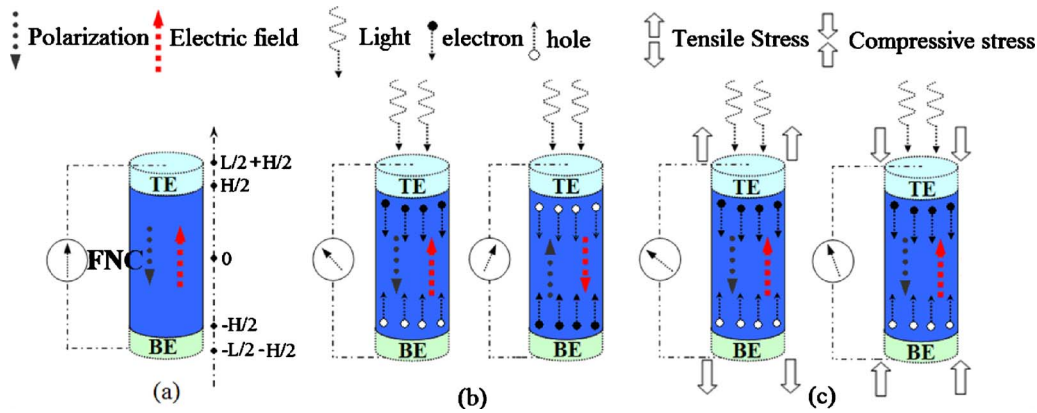


FIG. 1. (Color online) Schematic illustration of the FNC, (a) sandwiched between the top electrode (TE) and bottom electrode (BE) with the short-circuit boundary conditions, (b) the mechanism of the photocurrent generation for the two possible orientations of the polarization down, and up relative to the top electrode, (c) the photocurrent can be adjusted under the external compressive and tensile stress loads.

near the para/ferroelectric transition region.^{43–49} It then follows that the FPV effects in a FNC should also be sensitive to the external applied stress, and give rise to a piezophotovoltaic (PPV) effect that couples the photocurrent with mechanical loading. The aim of the present paper is to investigate the feasibility of such an effect. A simple model is constructed, in which the internal depolarization field driving the photoelectric current is calculated using a thermodynamic model based on the Ginzburg–Landau-type free energy functional. The photocurrent in a UV-illuminated FNC is calculated as functions of sample dimensions and applied stress. Using the PLZT FNC as an example, the efficiency and usefulness of the PPV effect is evaluated.

II. THE PHYSICAL MODEL

A FNC sample is sandwiched between short-circuited (SC) metal electrodes, and with length H and radius R as shown in Fig. 1(a). We assume in the present paper that all vector fields in the FNC, such as polarization and electric field, are along the z -direction. The FNC is illuminated from the top electrode, and the incident light is parallel or antiparallel to the polarization. We note that direction of the light can also be controlled by its polarization.¹⁵ Free charge carriers generated by the illumination are driven by the internal electric field in the FNC to produce an electric current [see Fig. 1(b)], which can be changed by applying an external mechanical load [see Fig. 1(c)]. To facilitate discussion, we classify the FNC according to $H < 0.5R$ (ND), $0.5R \leq H < 4R$ (NR), and $H > 4R$ (NW).

In the case of ferroelectric nanodisks (FNDs) where the sample radius is very large, i.e., $R \gg H$, the sample can be considered as a ferroelectric thin films (FTFs) of largely extend in the x -direction and y -direction. Based on previous works by Razeghi and Rogalski⁵⁰ and Qin *et al.*,^{20–23} the carrier concentrations n and p then obey the following conservation equations:

$$\begin{cases} \frac{dn}{dt} = \frac{1}{q} \frac{dJ_n}{dz} + G - A, \\ \frac{dp}{dt} = \frac{1}{q} \frac{dJ_p}{dz} + G - A, \end{cases} \quad (1)$$

where t is the time, q , the electronic charge, and z , the depth from the top surface of the FNC (Fig. 1). J_n and J_p are, respectively, the electron-current and hole-current densities. G is the generation rate of the electron-hole pairs from the photon flux and A is the annihilation rate due to the recombination. In most cases, the FPV effect is produced by UV-induced electrons and holes, with particle fluxes composed of diffusion and drift contributions, i.e., $q^{-1}J_n = D_n dn/dz + \mu_n nE$ and $-q^{-1}J_p = D_p dp/dz - \mu_p pE$, where D_n and μ_n are, respectively, the diffusivities and mobility of the electron, D_p and μ_p are the corresponding properties of the hole. E is the internal electric field.

Absent an external electric field, the applied electric field is entirely due to the depolarization field, i.e., $E = E_d$, which is determined by the spontaneous polarization and interface effects. The short-circuit current is given by $I_{sc} = A_0 J_{sc}$, where A_0 is the top electrode area, J_{sc} is the photocurrent density. Here J_{sc} can be written as a function of temperature T , quantum efficiency β , incident photon flux density φ , transmittance of the electrodes T_{ele} , and electron τ_n and hole τ_p lifetimes. The photocurrent has been derived using an approximate solution of Eq. (1), and is given by,²³

$$I_{sc} \approx \frac{A_0 \beta \alpha \varphi T_{Au}}{[\tau_n \mu_n (qE_d - \alpha kT)]^{-1} + \alpha/q} \exp(-\alpha H), \quad (2)$$

where α is the optical absorption coefficient and k is Boltzmann constant. Note that the depolarization field E_d in Eq. (2) was assumed to be uniform, neglecting effects due to the interface between metal electrodes and ferroelectric layer in previous works.^{20–23}

We consider as our thermodynamic reference a crystal of infinite extent (surfaceless) absent an applied field. Let P be the spontaneous polarization field (simply referred to as the polarization in the following).^{44–48} In general, the depolarization field E_d has two components, one coming from the incomplete charge compensation in the electrodes, and the

other from the inhomogeneity of the polarization field near the interface. The first component can be formulated in terms of the screening length l_s in the electrodes,^{32,51–56} where $l_s^2 \approx (3/8\pi)^2(h^2\varepsilon_e/3q^2m^*n_0^{1/3})$, h , the Planck constant, ε_e , the dielectric constant of the electrode, m^* , the electron effective mass in electrode and n_0 , the mean electron density at zero electric field. The second component is more complex and is determined by several factors, including space and surface charges, the small size effect, interface effect or Schottky barriers etc.^{8,27–32,46,57–61} The effects of the surface and interface on the profile of the depolarization field in the FNC and FTF have been discussed in previous works.^{34,35,42,53} In general, the profile of the depolarization field is nonuniform near the interfaces, and can be opposite to those at the center of the FNC and FTF.

Following Mehta⁵¹ and our previous work,⁴⁶ the internal electric field and compensation charges in the top and bottom electrodes for the “down” polarization state [Fig. 1(a)] are given by,

$$E_{eT}(z) = -q_e \sinh\left(\frac{L-2z}{2l_{sT}}\right) \times \left[\varepsilon_{eT} \sinh\left(\frac{L-l}{2l_{sT}}\right) \right]^{-1}, \quad \text{for } H/2 \leq z \leq L/2 + H/2,$$

$$E_{eB}(z) = q_e \sinh\left(\frac{L+2z}{2l_{sB}}\right) \left[\varepsilon_{eB} \sinh\left(\frac{L-l}{2l_{sB}}\right) \right]^{-1}, \quad \text{for } -L/2 - H/2 \leq z \leq -H/2, \quad (3)$$

where ε_{eT} , ε_{eB} and l_{sT} , l_{sB} are, respectively, the dielectric constants and screening lengths in the top and bottom electrodes, q_e is the compensation charge density in the electrodes, $L/2 - H/2$ is the thickness of the electrodes. Absent an external electric field, the internal electric field in the FNC can be derived via the Maxwell's equations,^{1,8,27,32,47} and is related to the depolarization field by $E_d(z) = -[P(z) + q_e]/\varepsilon_b$ for $-H/2 \leq z \leq H/2$, here ε_b is the background dielectric constant of ferroelectrics.^{44–48,51,56}

In the following, we assume that the top and bottom electrodes are the same, i.e., $\varepsilon_{eT} = \varepsilon_{eB} = \varepsilon_e$ and $l_{sT} = l_{sB} = l_s$, respectively. When $R \gg H$, the condition $\int_{-L/2}^{L/2} E(z) dz = \int_{-L/2}^{L/2} [E_{eT}(z) + E_d(z) + E_{eB}(z)] dz = 0$ must be satisfied for the short-circuit boundary condition. Taking into account size and interfacial effects, the depolarization field E_d is given by^{46,51–55}

$$E_d(z) = -\frac{P(z) + q_e}{\varepsilon_b} = -\frac{1}{\varepsilon_b} \left[P(z) - \frac{H/\varepsilon_b}{2l_s/\varepsilon_e + H/\varepsilon_b} \langle P \rangle \right], \quad (4)$$

here the compensation charge density can be derived as $q_e = \langle P \rangle = \frac{1}{V} \iiint_V P dv$ under conditions of electrostatic equilibrium,⁴⁷ $\langle P \rangle$ is the average polarization and V is the volume. We note that approximations of the depolarization field in the FNC have been derived,^{34,37,42} based on the assumption of complete charge compensation in the electrodes. Equation (4) is a more general expression for the inhomogeneous

depolarization field E_d in the FNC, taking into account both the incomplete charge compensation and inhomogeneous polarization field near the surface and interfaces. For the cylindrical geometry, Eq. (4) can be approximated by

$$E_d(r, z) \approx -\frac{\eta(H, R)}{\varepsilon_b} \left[P(r, z) - \frac{H/\varepsilon_b}{2l_s/\varepsilon_e + H/\varepsilon_b} \langle P \rangle \right], \quad (5)$$

where $\eta(R, h)$ can be estimated using the relation $\eta(R, L) \approx 1/\left[1 + \left(\frac{h}{2R}\right)^2\right]$.³⁴

The depolarization field $E_d(r, z)$ in Eq. (5) has to be solved self-consistently with $P(r, z)$ across the paraferroelectric phase boundary. A proven effective approach is via a thermodynamic formulation based on a Ginzburg–Landau-type free energy functional.^{34,35,37,43,46,47} Taking into account effects of the surface tension, interface, surface, depolarization field and uniform external applied stress σ_z , the total free energy for the FNC can be written as,^{34,46,56}

$$F = 2\pi \int_{-H/2}^{H/2} dz \int_0^R r dr \left\{ \left[\frac{\alpha_0}{2} (T - T_{c0}) - 2Q_{12} \sigma_s(\mu, R) - Q_{11} \sigma_z \right] P^2(r, z) + \frac{\beta}{4} P^4(r, z) + \frac{\gamma}{6} P^6(r, z) + \frac{g}{2} [\nabla P(r, z)]^2 - (s_{11} + s_{12}) \sigma_s^2(\mu, R) - \frac{1}{2} s_{11} \sigma_z^2 - 2s_{12} \sigma_s(\mu, R) \sigma_z - P E_d - \frac{1}{2} \varepsilon_b E_d^2 \right\} + F_{s-w} + F_{\text{Interface}}, \quad (6)$$

where α_0 , β , γ , η , and g are the expansion coefficients of the free energy of the reference crystal, and T_{c0} is the corresponding Curie–Weiss temperature. Q_{ij} are the electrostrictive coefficients. $\sigma_s(\mu, R)$ is the uniform compressive radial stress induce by the surface tension, given by $\sigma_s(\mu, R) = -\mu/R$.^{34,42,57} μ is the effective surface tension coefficient. σ_z is the external applying stress along z direction determined by the external applying force f , and $\sigma_z = f/(\pi R^2)$. F_{s-w} is the energy solely determined by the surface effect of the cylindrical sidewall. $F_{\text{Interface}}$ is the energy associated with effect of the planar end interfaces, and is due to contributions from the a myriad of contributions, including space and surface charges, size effect, interface effect or Schottky barriers. Different theoretical models have been established to investigate the effects of the interface on the internal electric field near the interface of the MFM system.^{8,32} In this work, we adopt conventional models, in which F_{s-w} and $F_{\text{Interface}}$ are empirically represented, respectively, as $F_{s-w} = 2\pi R g / \delta_{s-w} \int_{-H/2}^{H/2} P^2|_{r=R} dz$ and $F_{\text{Interface}} = 2\pi g \int_0^R (\delta_{T-T}^{-1} P^2|_{z=H/2} + \delta_{T-T}^{-1} P^2|_{z=-H/2}) r dr$.^{34,42} Here δ_{s-w} is an extrapolation length due to the surface effect of the cylindrical sidewall,^{34,35} δ_{T-T} and δ_{T-T} are extrapolation lengths that should take into account effects on the distribution of the polarization due to space and surface charges, interface effect or Schottky barriers etc. of the top and bottom interfaces.^{8,30,32,57–61} In the present work, the extrapolation lengths of the top and bottom interface are same, i.e., $\delta_{T-T} = \delta_{T-T} = \delta_T$.⁶¹ Note that δ_{T-T} and δ_{T-T} have different physical origins, such as different top-bottom electrodes, interface effect and polarization switching

etc., which may be obtained from first-principle calculations^{8,52,55} and a combination of first-principle and phenomenological calculations.^{57,58}

At equilibrium, the polarization P and depolarization field E_d at a fixed temperature and electromechanical boundary conditions are related through the stationary solutions of the Euler–Lagrange equation,^{31,32,46} i.e.,

$$\delta F / \delta P = 0, \quad (7)$$

here the corresponding boundary conditions due to the surface and interface effects are expressed as $\partial P / \partial r = -P / \delta_{s-w}$ for $r=R$, and $\partial P / \partial z = \mp P / \delta_l$, for $z = \pm H/2$. In this way, solutions of the polarization P and depolarization field E_d of the FNC can be obtained numerically as functions of the sample dimensions and external mechanical load.

Expressing the depolarization field as functions of length H , radius R and external applied stress σ_z , the photocurrent for the FNC from Eq. (2) can be approximately rewritten as,

$$I_{sc} \approx \frac{\pi R^2 \beta \alpha \varphi T_{ele}}{\{\tau_n \mu_n [q \bar{E}_d(H, R, \sigma_z) - \kappa \alpha k T]\}^{-1} + \kappa \alpha / q} \exp(-\alpha H), \quad (8)$$

where $\bar{E}_d(H, R, \sigma_z) = V^{-1} \int \int \int V E_d(r, z) dV$ is the mean depolarization field, obtained from the numerical solution of Eqs. (5)–(7). Schematics of the internal depolarization field across the FNC z and x axes are similar to results in Ref. 34. Here κ takes on the value of 1 or -1 according to whether the polarization field is directed down (i.e., $\bar{E}_d > 0$) or “up” (i.e., $\bar{E}_d < 0$).

III. RESULTS AND DISCUSSIONS

The study in this paper is conducted for PLZT which is one of the most promising candidates for ferroelectric-based photovoltaic applications, and has been successfully fabricated and implemented recently. We consider a PLZT FNC sandwiched between Au top-bottom electrodes with the short-circuit boundary conditions. To focus on the PPV effect of the FNC we consider a fixed radius of $R=50$ nm, for which the surface energy and surface tension effects are negligible.^{34,42,61} We note that when the radius or length of the FNC is less than 10 nm, the surface energy and surface tension effects becomes important, which have been comprehensively discussed.^{34,42}

Values of the expansion coefficients of the free energy, electrostrictive coefficients, elastic properties and background dielectric constant are obtained from the literature.^{44,45,62–64} We use the extrapolation lengths obtained in previous works^{34,42} which are only approximated, for future calculations, values obtained from the first-principle-based calculations⁵⁷ or first-principle-phenomenological⁵⁸ calculations may provide a more reliable input database. Other parameters used in our calculations are:^{23,65,66} $k = 1.38 \times 10^{-23}$ J/K; $q = 1.6 \times 10^{-19}$ C; $\beta = 1.06 \times 10^{-3}$; $T_{ele} = 0.6$; $\tau_n = \tau_p = 200$ ps; $\alpha = 2 \times 10^4$ cm⁻¹; $\mu_n = 3$ cm²/V s; $\mu_p = 2.93 \times 10^{-6}$ cm²/V s; $l_s = 0.5 \times 10$ Å; $\varepsilon_e = 8\varepsilon_0$; $\varepsilon_0 = 8.85 \times 10^{-12}$ F/m.

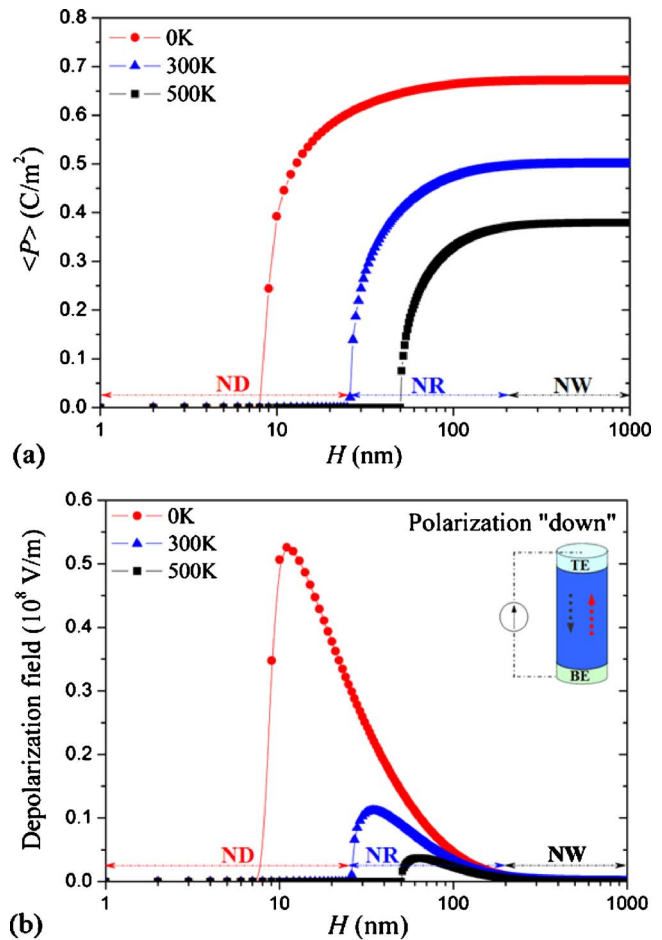


FIG. 2. (Color online) (a) The average polarization vs the length of the FNC and (b) the average internal depolarization field vs the length of the FNC for polarization down.

We first consider an unilluminated and unstressed FNC under short-circuit boundary conditions. Directions of the polarization and internal depolarization field are as shown in Fig. 1(a). Solving Eq. (7), the average polarization $\langle P \rangle$ as a function of sample length H is plotted in Fig. 2(a) for temperatures $T=0, 300$, and 500 K. Temperature-dependent critical lengths H_c of 8 nm for 0 K, 26 nm for 300 K, and 50 nm for 500 K can be seen, below which the FNC is paraelectric, and above, it is ferroelectric. In the ferroelectric region, the spontaneous polarization P behaves almost like a step function, increasing sharply with H and quickly saturating near the bulk polarization values. Figure 2(b) shows \bar{E}_d as a function of sample geometry and temperature. \bar{E}_d can be seen to be negligible when the length H of the FNC is either too large or too small. The peak depolarization field \bar{E}_d^{\max} at room temperature is only 1/4 of \bar{E}_d^{\max} at 0 K, but is more than four times larger than \bar{E}_d^{\max} at 500 K.

In the static polarization state¹⁰ and neglecting the asymmetric interfacial effects,^{67,68} Fig. 3 shows the normalized photocurrent I_{sc}/I_{sc}^0 as a function of specimen length H at room temperature. Here I_{sc}^0 is the diffusion component of the photocurrent, i.e., $I_{sc}^0 = I_{sc}|_{\bar{E}_d=0}$, and I_{sc} is obtained by solving Eqs. (7) and (8). Figure 3 suggests that the polarization state of the poled memory cell can be nondestructively read out

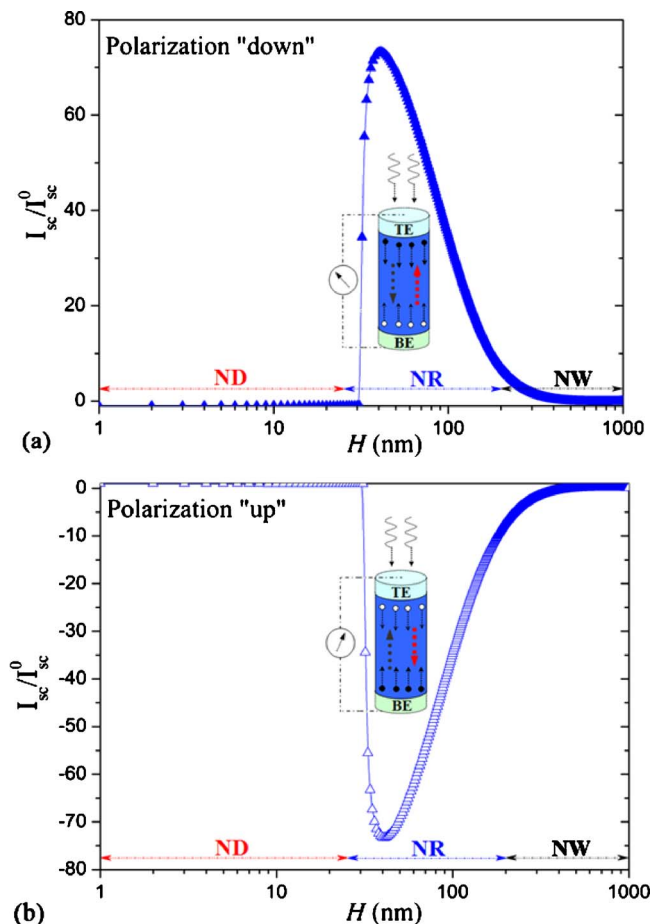


FIG. 3. (Color online) The normalized photocurrent of the FNC for the polarization (a) down and (b) up at room temperature.

using light illumination.^{10,14,15} We note that although this feasibility has been confirmed by many investigations in FTF capacitors with the short-circuit conditions, similar information to facilitate the use of FNCs as FPV nanodevices has not been available.

As discussed earlier in this paper, the application of an external stress is expected to affect the polarization state of the FNC, producing a PPV effect [see Fig. 1(c)]. Numerically solving Eqs. (5) and (7) with the boundary conditions, the resulting average polarization and depolarization fields and I_{sc}/I_{sc}^0 at room temperature (300 K) are shown as functions of H for different external stresses in Figs. 4(a)–4(c). Comparing Fig. 4(a) with the 300 K curve in Fig. 2(a), it can be seen that the application of a tensile stress reduces the critical lengths H_c and raises the average polarization $\langle P \rangle$ in a PLZT FNC, and a compressive stress has the opposite effect. Figures 4(b) and 4(c) show that the application of a tensile stress above the critical length H_c increases both the average depolarization field \bar{E}_d and the photocurrent I_{sc} . This increase is very sensitive to the specimen geometry. Thus, for lengths H between 20 and 26 nm, application a tensile stress of $\sigma_z=0.3$ GPa may increase the photocurrent by a huge amount of ~ 100 times. Between 30 and 50 nm, application of a compressive stress of $\sigma_z=-0.3$ GPa can reduce the photocurrent by a similarly huge amount of ~ 80 times.

To facilitate discussions in the following, we focus on

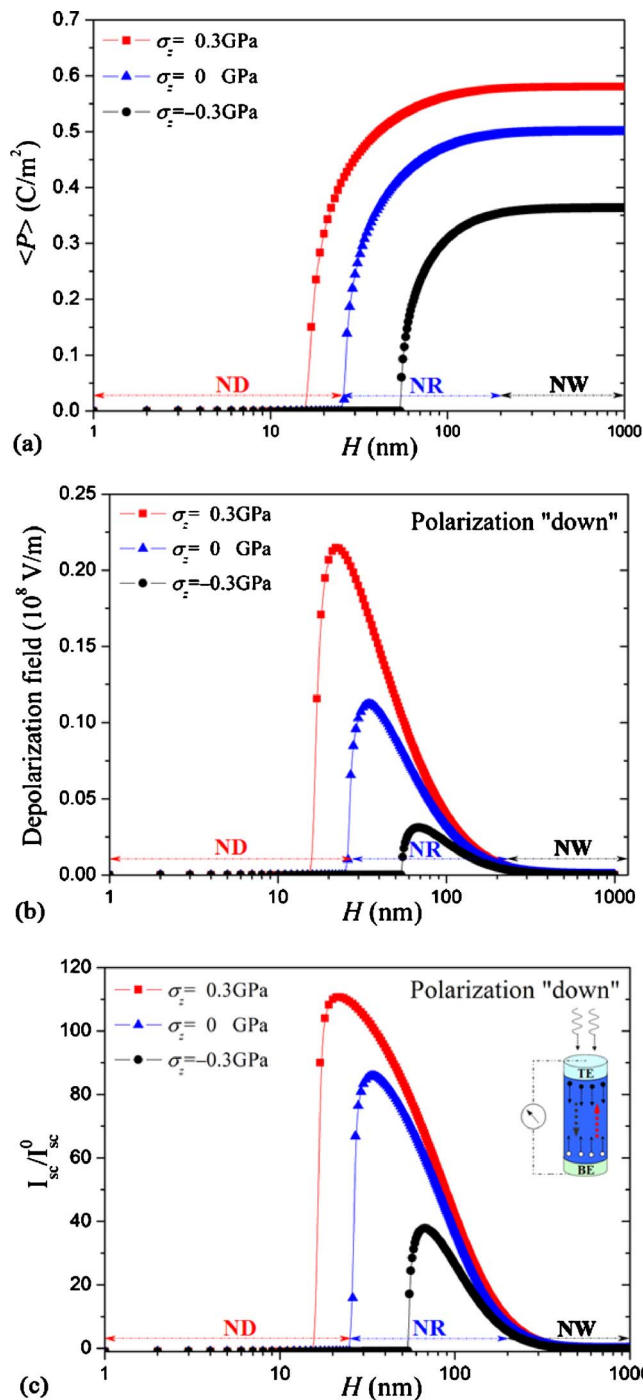


FIG. 4. (Color online) (a) The average polarization, (b) internal depolarization field, and (c) normalized photocurrent of the FNC as function of the length with compressive and tensile stress loads.

FNCs with H/R ratios of 4, 1, and 1/4, corresponding to the respective geometries of the typical NW, NR, and ND. We also adopt the convention that compressive stresses are negative, and tensile stresses are positive. Figure 5(a) shows $\langle P \rangle$ as a function of the applied stress σ_z at room temperature (300 K). It is clear that critical stresses σ_c exists for all geometries, on the tensile side of which the FNC is ferroelectric, and on the compressive side of which, the FNC becomes paraelectric. The critical stress σ_c is a function of the H/R ratio, decreasing toward the compressive side as H/R increases. Thus, for the typical ND with $H/R=0.25$, σ_c is ten-

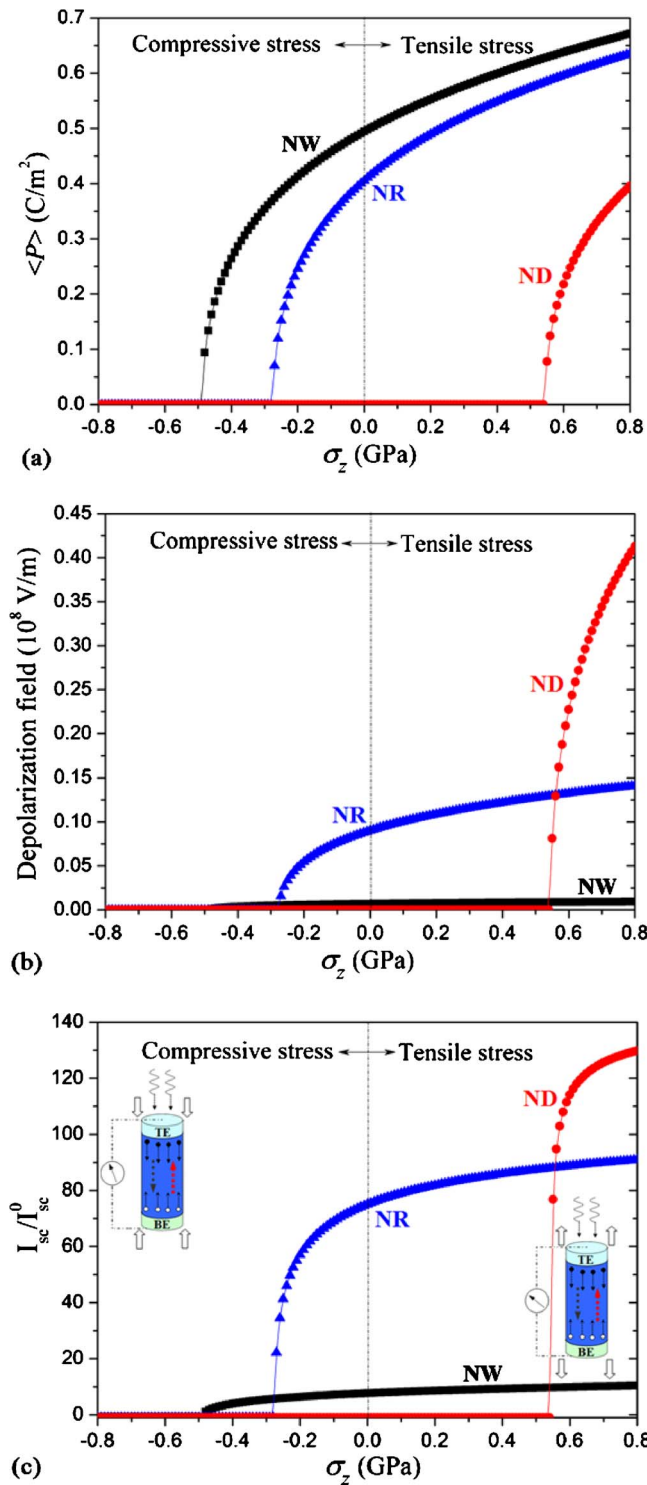


FIG. 5. (Color online) (a) The average polarization, (b) internal depolarization field, and (c) normalized photocurrent of the ferroelectric ND, NR, and NW as function of the applied stress loads, respectively.

sile with a magnitude of 0.54 GPa. For the typical NR with $H/R=1$, σ_c is compressive and is equal to -0.28 GPa, and for the typical NW with $H/R=4$, σ_c is more compressive at -0.5 GPa. Figure 5(b) shows the average depolarization field as a function of the applied stress. For the typical NW, this field remains less than 10 kV/cm for whole range of σ_z under consideration, from -0.5 to 0.8 GPa. We note that this range of the applied stress correspond to a mechanical force

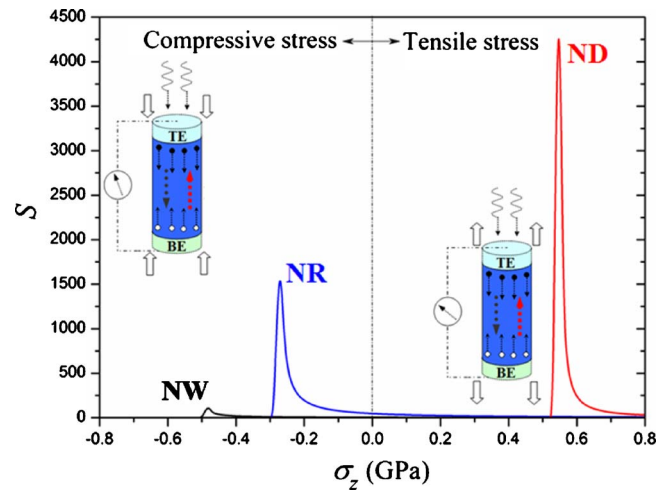


FIG. 6. (Color online) The stress sensitivity S of the photocurrent measures the magnification in the photocurrent due to a relative change in the applied stress.

from -4.0 to $6.3 \mu\text{N}$ for a FNC with a radius of 50 nm. With the same applied stress, the depolarization field for the NR and ND geometries can be seen to vary over a large range of well over an order of magnitude.

The normalized photocurrents I_{sc}/I_{sc}^0 are plotted in Fig. 5(c) as functions of the applied uniaxial stress. It can be seen that in all cases the photocurrent increases as the applied stress becomes more tensile. The PPV effect is found to be highly sensitive to the applied stress in a region of about 100 MPa near σ_c . An order-of-magnitude change in the photocurrent can be produced in this region with a change in stress of just a few percent. In Fig. 6, we plot the stress sensitivity of the photocurrent $S=(\sigma/I_{sc}^0)(dI_{sc}/d\sigma)$, which measures the magnification in the photocurrent due to a relative change in the applied stress, i.e., $(\Delta I_{sc}/I_{sc}^0)=S(\Delta\sigma/\sigma)$. It can be seen that S may magnify a stress signal by hundreds of times in a region near σ_c which is adjustable via the sample geometry, such as the H/R ratio.

Although the present study is based on PLZT which is one of the most promising candidates for ferroelectric-based photovoltaic applications, the BFO system may provide a much larger photocurrent than PLZT thin films.¹⁵ In this regard, BFO or $\text{PTO}_x\text{BFO}_{1-x}$ etc may be used to make FNCs in photovoltaic or PPV nanodevices of even higher sensitivity.

IV. CONCLUSIONS

In summary, the effects of applied stress on the photoelectricity in a ferroelectric nanocylinder (FNC) sandwiched between SC metal electrodes have been investigated. The internal depolarization field determined by the spontaneous polarization that drives the photoelectric current is calculated using a thermodynamic model based on the Ginzburg–Landau-type free energy functional. The PPV effect is found to be highly sensitive to the applied stress near the stress-induced para/ferroelectric phase transition. An ultra sensitive stress regime exists, in which a few percent change in the applied stress can be magnified into hundreds of times in the change in the photocurrent. That the stress regimes in which this occurs can be adjusted by varying the dimensions of the

FNC makes this phenomenon even more interesting. This effect offers a good potential for applications in HSPMS, memories, switchable nanodevices, or other photovoltaic nanodevices.

ACKNOWLEDGMENTS

This project was supported by grants from the Research Grants Council of the Hong Kong Special Administrative Region (Grant Nos. G-YX0T, 5322/04E, and N53408). Y. Zheng is also grateful for support from the National Science Foundation of China (Grant Nos. 10902128, 10732100, and 10831160504).

- ¹M. E. Lines and A. M. Glass, *Principle and Applications of Ferroelectrics and Related Materials* (Clarendon, Oxford, 1977).
- ²S. M. Sze, *Principle of Semiconductor Devices*, 2nd ed. (Wiley, New York, 1981).
- ³V. M. Fridkin, *Photoferroelectrics* (Springer-Verlag, Berlin, 1979).
- ⁴A. G. Chynoweth, *Phys. Rev.* **102**, 705 (1956).
- ⁵F. S. Chen, *J. Appl. Phys.* **40**, 3389 (1969).
- ⁶A. M. Glass, D. von der Linde, and T. J. Negran, *Appl. Phys. Lett.* **25**, 233 (1974).
- ⁷H. Presting and R. Von Baltz, *Phys. Status Solidi B* **112**, 559 (1982).
- ⁸M. Dawber, K. M. Rabe, and J. F. Scott, *Rev. Mod. Phys.* **77**, 1083 (2005).
- ⁹L. Pintilie, M. Alexe, A. Pignolet, and D. Hesse, *Appl. Phys. Lett.* **73**, 342 (1998).
- ¹⁰L. Pintilie, I. Vrejoiu, G. L. Rhun, and M. Alexe, *J. Appl. Phys.* **101**, 064109 (2007).
- ¹¹A. Matsumura, Y. Kamaike, T. Horiuchi, M. Shimiz, T. Shiosaki, and K. Matsushige, *Jpn. J. Appl. Phys., Part 1* **34**, 5258 (1995).
- ¹²V. K. Yarmarkin, B. M. Gol'tsman, M. M. Kazanin, and V. V. Lemanov, *Phys. Solid State* **42**, 522 (2000).
- ¹³G. G. Zheng, J. Xu, L. Fang, M. R. Shen, and X. L. Wu, *Appl. Phys. Lett.* **93**, 172101 (2008).
- ¹⁴A. Kholkin, O. Boiarkine, and N. Setter, *Appl. Phys. Lett.* **72**, 130 (1998).
- ¹⁵T. Choi, S. Lee, Y. J. Choi, V. Kiryukhin, and S. W. Cheong, *Science* **324**, 63 (2009).
- ¹⁶P. Pooanaas, A. Dogan, S. Thakoor, and K. Uchino, *J. Appl. Phys.* **84**, 1508 (1998).
- ¹⁷K. Nonaka, M. Akiyama, T. Hagio, and A. Takase, *Jpn. J. Appl. Phys., Part 1* **34**, 2344 (1995).
- ¹⁸M. Ichiki, R. Maeda, Y. Morikawa, Y. Mabune, T. Nakada, and K. Nonaka, *Appl. Phys. Lett.* **84**, 395 (2004).
- ¹⁹M. Ichiki, Y. Morikawa, Y. Mabune, T. Nakada, K. Nonaka, and R. Maeda, *J. Phys. D: Appl. Phys.* **37**, 3017 (2004).
- ²⁰M. Qin, K. Yao, and Y. C. Liang, *Appl. Phys. Lett.* **93**, 122904 (2008).
- ²¹M. Qin, K. Yao, Y. C. Liang, and B. K. Gan, *Appl. Phys. Lett.* **91**, 092904 (2007).
- ²²M. Qin, K. Yao, and Y. C. Liang, *J. Appl. Phys.* **105**, 061624 (2009).
- ²³M. Qin, K. Yao, Y. C. Liang, and S. Shannigrahi, *J. Appl. Phys.* **101**, 014104 (2007).
- ²⁴B. K. Gan, K. Yao, S. C. Lai, Y. F. Chen, and P. C. Goh, *IEEE Electron Device Lett.* **29**, 1215 (2008).
- ²⁵Y. B. Tang, Z. H. Chen, H. S. Song, C. S. Lee, H. T. Cong, H. M. Cheng, W. J. Zhang, I. Bello, and S. T. Lee, *Nano Lett.* **8**, 4191 (2008).
- ²⁶K. Seeger, *Semiconductor Physics: An Introduction*, 9th ed. (Springer, Berlin, 2004).
- ²⁷J. F. Scott, *Ferroelectric Memories* (Springer, Berlin, 2000).
- ²⁸G. Gerra, A. K. Tagantsev, N. Setter, and K. Parlinski, *Phys. Rev. Lett.* **96**, 107603 (2006).
- ²⁹L. Pintilie and M. Alexe, *J. Appl. Phys.* **98**, 124103 (2005).
- ³⁰C. G. Duan, R. F. Sabirianov, W. N. Mei, S. S. Jaswal, and E. Y. Tsymlal, *Nano Lett.* **6**, 483 (2006).
- ³¹B. Wang and C. H. Woo, *J. Appl. Phys.* **97**, 084109 (2005).
- ³²A. K. Tagantsev, V. O. Sherman, K. F. Astafiev, J. Venkatesh, and N. Setter, *J. Electroceram.* **11**, 5 (2003).
- ³³W. L. Zhong, Y. G. Wang, P. L. Zhang, and B. D. Qu, *Phys. Rev. B* **50**, 698 (1994).
- ³⁴A. N. Morozovska, E. A. Eliseev, and M. D. Glinchuk, *Phys. Rev. B* **73**, 214106 (2006).
- ³⁵A. N. Morozovska, E. A. Eliseev, and M. D. Glinchuk, *Physica B* **387**, 358 (2007).
- ³⁶I. I. Naumov and H. X. Fu, *Phys. Rev. Lett.* **95**, 247602 (2005).
- ³⁷Y. Zheng, C. H. Woo, and B. Wang, *J. Phys. Condens. Matter* **20**, 135216 (2008).
- ³⁸Y. F. Gao and Z. L. Wang, *Nano Lett.* **7**, 2499 (2007).
- ³⁹Z. L. Wang and J. H. Song, *Science* **312**, 242 (2006).
- ⁴⁰X. D. Wang, J. H. Song, J. Liu, and Z. L. Wang, *Science* **316**, 102 (2007).
- ⁴¹Z. Y. Wang, J. Hu, A. P. Suryavanshi, K. Yum, and M. F. Yu, *Nano Lett.* **7**, 2966 (2007).
- ⁴²Y. Zheng, C. H. Woo, and B. Wang, *Nano Lett.* **8**, 3131 (2008).
- ⁴³L. D. Landau, E. M. Lifshitz, and L. P. Pitaevskii, *Electrodynamics of Continuous Media* (Oxford University Press, London, 1984).
- ⁴⁴J. Wang and T. Y. Zhang, *Phys. Rev. B* **73**, 144107 (2006).
- ⁴⁵S. Y. Hu, Y. L. Li, and L. Q. Chen, *J. Appl. Phys.* **94**, 2542 (2003).
- ⁴⁶Y. Zheng and C. H. Woo, *Nanotechnology* **20**, 075401 (2009).
- ⁴⁷C. H. Woo and Y. Zheng, *Appl. Phys. A: Mater. Sci. Process.* **91**, 59 (2008); Y. Zheng and C. H. Woo, *ibid.* **97**, 617 (2009).
- ⁴⁸A. N. Morozovska, V. K. Sergei, A. E. Eliseev, V. Gopalan, and S. V. Svechnikov, *Phys. Rev. B* **78**, 125407 (2008).
- ⁴⁹A. K. Tagantsev, *Ferroelectrics* **375**, 19 (2008).
- ⁵⁰M. Razezghi and A. Rogalski, *J. Appl. Phys.* **79**, 7433 (1996).
- ⁵¹R. R. Mehta, B. D. Silverman, and J. T. Jacobs, *J. Appl. Phys.* **44**, 3379 (1973).
- ⁵²J. Junquera and P. Ghosez, *Nature (London)* **422**, 506 (2003).
- ⁵³Y. Zheng, M. Q. Cai, and C. H. Woo, *Acta Mater.* **58**, 3050 (2010).
- ⁵⁴A. N. Morozovska, E. A. Eliseev, S. V. Svechnikov, Y. Li, S. V. Svechnikov, V. Y. Shur, P. Maksymovych, V. Gopalan, L.-Q. Chen, and S. V. Kalinin, *Phys. Rev. B* **80**, 214110 (2008).
- ⁵⁵D. J. Kim, J. Y. Jo, Y. S. Kim, Y. J. Chang, J. S. Li, J. G. Yoon, T. K. Song, and T. W. Noh, *Phys. Rev. Lett.* **95**, 237602 (2005).
- ⁵⁶A. Y. Emelyanov, N. A. Pertsev, and A. L. Kholkin, *Phys. Rev. B* **66**, 214108 (2002).
- ⁵⁷G. Gerra, A. K. Tagantsev, and N. Setter, *Phys. Rev. Lett.* **98**, 207601 (2007).
- ⁵⁸C. G. Duan, S. S. Jaswal, and E. Y. Tsymlal, *Phys. Rev. Lett.* **97**, 047201 (2006).
- ⁵⁹N. A. Pertsev and R. Dittmann, *J. Appl. Phys.* **101**, 074102 (2007).
- ⁶⁰N. A. Pertsev and H. Kohlstedt, *Phys. Rev. Lett.* **98**, 257603 (2007).
- ⁶¹R. Kretschmer and K. Binder, *Phys. Rev. B* **20**, 1065 (1979).
- ⁶²K. J. Uchino, E. J. Sadanaga, and T. Hirose, *J. Am. Ceram. Soc.* **72**, 1555 (1989).
- ⁶³M. J. Haun, E. Furman, H. A. McKinstry, and L. E. Cross, *Ferroelectrics* **99**, 27 (1989).
- ⁶⁴N. A. Pertsev, V. G. Kukhar, H. Kohlstedt, and R. Waser, *Phys. Rev. B* **67**, 054107 (2003).
- ⁶⁵K. Rabe, C. H. Ahn, and J. M. Triscone, *Physics of Ferroelectrics: A Modern Perspective* (Springer, Berlin, 2007).
- ⁶⁶T. B. Charles and J. W. Jeffrey, *IEEE Trans. Electron Devices* **46**, 776 (1999).
- ⁶⁷Y. S. Yang, S. J. Lee, S. Yi, B. G. Chae, S. H. Lee, H. J. Joo, and M. S. Jang, *Appl. Phys. Lett.* **76**, 774 (2000).
- ⁶⁸O. G. Vendik, S. P. Zubko, and N. Y. Medvedeva, *J. Appl. Phys.* **105**, 053515 (2009).